Regulating Orbital Decay through Passive Thermochromism in PMPEs for Orbital Debris Remediation

Joseph Ivarson
Auburn University
141 Engineering Dr
Auburn, AL, 36849
jti0002@auburn.edu

John Mulvaney
NASA Langley Research Center
Space Mission Analysis Branch
Hampton, Virginia, 23681

Andrew Sais
NASA Langley Research Center
Space Mission Analysis Branch
Hampton, Virginia, 23681

Davide Guzzetti
Auburn University
141 Engineering Dr
Auburn, AL, 36849
dzg0029@auburn.edu

Abstract*—Current state-of-the-art techniques for small debris (<1 cm) remediation use dust clouds composed of small grains to induce artificial drag and deorbit debris. By passively controlling the variation of particle properties, it is possible to harness external forces to steer orbital motion. Programmable Metamaterial Particle Ensembles (PMPEs) could enable more precise regulation of semi-major axis variations, hence improving management of radial dispersion, along-track dispersion, and orbital decay compared to inert dust clouds. This work investigates how solar radiation pressure (SRP) can be utilized for orbit control by regulating optical properties according to temperature. Preliminary studies of the PMPE design space were performed using a thermo-orbit model to assess particle trajectories and temperature responses, and to begin informing the requirements for orbital debris removal technology development. Initial results demonstrated the intended effects of PMPEs, showing that variations in optical properties with temperature can induce SRP asymmetry, thereby enabling semi-major axis control over successive orbits. Subsequent analysis identified performance metrics, such as volumetric heat capacity, which could inform the optimal selection of materials to prolong the duration of asymmetric SRP induction. Further studies explored design parameters that maximize control authority over decay rates for specific test cases. In the orbit range of interest for small debris remediation (800 to 1000 km), we found that PMPEs have the capability to either cancel out or double the natural decay rates, enabling operators to optimize interactions with debris. This research highlights the promising potential of PMPEs for innovative passive orbit control solutions, paving the way for further advancements in space debris mitigation.

TABLE OF CONTENTS

979-8-3503-5597-0/25/$31.00 ©2025 IEEE

1. INTRODUCTION

The total amount of trackable objects (> 10 cm in diameter) in Earth orbit has more than doubled in the past 20 years, partially due to the substantial increase in fragmentation debris during that time [1], [2], [3]. The careful tracking of this debris gives capability for some spacecraft operators to conduct avoidance maneuvers while on orbit to escape the possible catastrophic effects of a collision. Unfortunately, there is a substantial population of debris that cannot be tracked, some of which is still large enough to deal a lethal blow to vital systems, endangering mission and/or crew. Much of this debris gathers at altitudes in the 800 to 1000 km range where the thin atmosphere exerts limited influence, resulting in debris lifespans of several decades [2], [3]. Recent cost and benefit analysis of orbital debris remediation suggests there are potential benefits to removing large quantities of small, untrackable debris (1 to 10 mm in diameter), which at the very least have the potential to degrade mission capability [2], [3]. Additionally, NASA's Space Technology Mission Directorate (STMD) has identified the remediation of small debris as an existing shortfall, highlighting the need for research in this area [4].

An existing concept for the remediation of small debris is the orbital or sub-orbital deployment of small tungsten grains in the form of a dust cloud. The ensuing collisions between debris and the cloud leads to an induced drag on small debris, accelerating their orbital decay to lower altitudes where atmospheric drag has a more dominating effect [5], [6], [7]. In orbit, the dust forms a ring that allows it to intercept a large number of small debris in an operationally simple manner. However, the particle design space is partially constrained by the decay rate of the dust particles, which are synced with the induced debris decay rate to maximize efficacy [6]. In this concept, we propose the orbital deployment of programmable metamaterial particle ensembles (PMPEs) to remediate small debris. By precisely tuning the geometrical, optical, thermal, and electromagnetic properties of each particle in response to environmental stimuli, we may gain control of the collective behavior of the PMPE cloud. This enables movement and dynamics that surpass what is achievable with the current state of the art, natural deorbiting with an inert particle based dust cloud. More specifically, we may gain control of PMPE descent or ascent rate, area-density, and lifespan on orbit, and we may expand the design space for the deployed cloud. These factors govern the velocity imparted on encountered debris as well as the number of encounters, both key metrics

in determining the remediation cost of debris. Enhanced control over the evolution of the dust cloud could significantly improve its remediation potential.

To further explore the potential of PMPEs, it is essential to introduce how smart materials can be leveraged for effective orbit regulation and debris remediation. Some metamaterials experience variations in optical properties in response to stimuli including temperature, presence of electric or magnetic field, and UV exposure [8]. While the PMPE design space could allow for passive regulation through solar radiation pressure (SRP) utilizing many types of smart materials, in this analysis, we focus on the variation of optical properties with temperature using thermochromic materials. With careful particle engineering, it is possible to regulate SRP acceleration by transition between a highly specularly reflective state and a state with diffuse reflection or absorption. That is, the key function of a PMPE optical transition is to generate an asymmetry in the SRP influence over successive orbits. Over time, this asymmetry modulates the effect of SRP on semi-major axis variation, leading to the capability to control the decay rate of the particle. For example, after emerging from eclipse, a particle is at its coolest temperature and the metamaterial coating is reflective. As the particle moves into sunlight, photons are reflected specularly, generating a "strong" SRP acceleration that decelerates the particle. At sun conjunction[1], the particle temperature surpasses the activation temperature, and the coating turns opaque; the number of photons that are specularly reflected drops. During the transition between sun conjunction and eclipse entry, the work produced by SRP is positive (i.e., it accelerates the particle). However, because reflectivity is reduced, the SRP acceleration is weaker than the deceleration experience on the cold side of the orbit, realizing an orbit energy depleting cycle; this case is illustrated in Figure 1. Note that the cycle can become energy-pumping by switching to a metamaterial coating that is opaque when cold and reflective when hot.

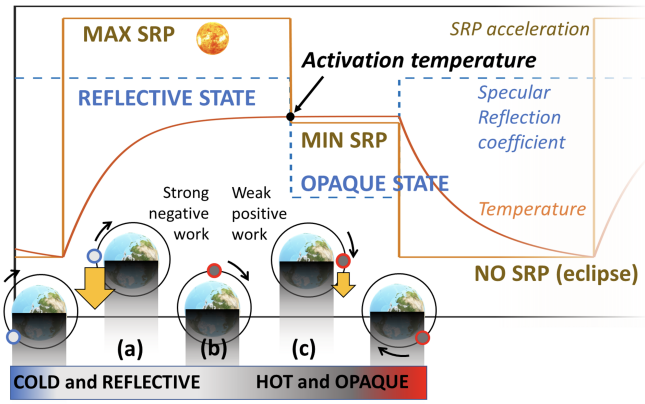

Figure 1. PMPE energy depletion or pumping is achieved through syncing optical property variation with particle motion by taking advantage of on-orbit eclipses

In this paper, we present the results of our preliminary exploration of the design space for thermochromic PMPEs. Section 2 details the construction of our thermo-orbit model used for single particle simulations. In Section 3, we examine the identified performance metrics and analyze their impact on the design. Section 4 provides the results of our study, along with other key findings relevant to the concept.

[1]This is a notional location, the actual orbit location of the thermochromic transition is determined by external heat flux values and particle properties.

2. THERMO-ORBIT MODELING

The thermo-orbit model was built in python and uses the two-body problem equations of motion including atmospheric drag and SRP in an Earth-centered inertial reference frame (ECI).

$$\ddot{\mathbf{r}} = -\frac{\mu}{r^3}\mathbf{r} - \frac{1}{2}\frac{\mathbf{C_d A_c}}{\mathbf{m}}\rho_\infty ||\mathbf{V_a}||\mathbf{V_a} - \frac{P_{srp} C_R(T_p) A_c \phi}{m}\hat{\mathbf{u}}_{\text{sun}} \quad (1)$$

Here, $\mathbf{r}$ is the particle position vector, $\mu = 3.986 \times 10^{14}$ m^3s^{-2}, m is particle mass in kg, $C_d = 2$ is the coefficient of drag, and A_c is the particle cross-sectional area in meters. The particle velocity relative to the atmosphere, $\mathbf{V_a} = \mathbf{V} - (\mathbf{\Omega_E} \times \mathbf{r})$ in m/s, is calculated based on position and Earth angular velocity Ω_E in rad/s. We employ the pynrlmsise00 [9] python package using the particle state to find density, ρ_∞ in kg/m^3, from the NRLMSISE00 model [10]. The current configuration uses NOAA products [11] to allow us to evaluate particle behavior under mean, minimum, and maximum solar effects over Solar Cycle 24, as well as capture diurnal variations in atmospheric density. We use $P_{srp} = 4.57\times10^{-6}$ N/m^2 from Vallado's formulation of SRP, and the coefficient of reflection, $C_R(T_p)$, is between 0 and 2 [12]; in our case, this value is dependent on thermochromic transition temperature. We use the cylindrical eclipse model described in Reference [13] to define when the particle is in sunlight ($\phi = 1$) or eclipse ($\phi = 0$), and we find the unit vector to the sun, $\hat{\mathbf{u}}_{sun}$, through triangulation between the particle state and the sun position from the eclipse model.

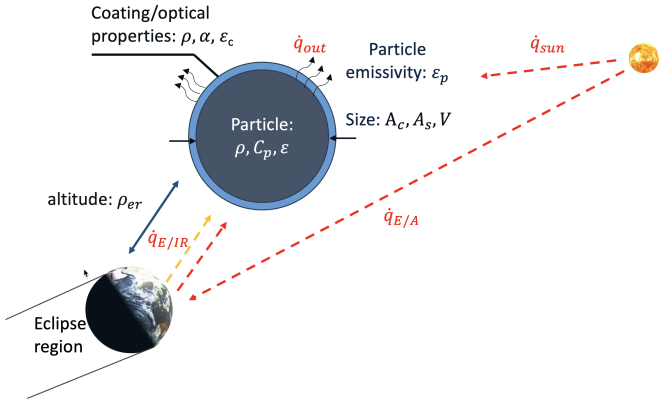

Figure 2. The design variables of the considered thermochromic PMPEs and the heat sources considered in this model

The SRP and eclipse models couple the particle's temperature and dynamics; on orbit thermal variation due to eclipse and lighting conditions leads to particle optical property changes from the thermochromic material. Temperature is included as a state variable with the heat diffusion equation as the governing law; as illustrated in Figure 2, we consider four heat sources, all expressed in W/m^2. First, we consider solar flux, $\dot{q}_{sun}$,

$$\dot{q}_{sun} = \frac{S}{R_{AU}^2}\alpha A_c \phi \quad (2)$$

where $S = 1361$ W/m^2 is the solar constant [14], $R_{AU} = 1$ is the distance of the particle to the Sun in astronomical units

(AU), α is the absorptivity of the particle, A_c is the cross-sectional area of the particle, and ϕ is the previously described binary eclipse factor. Secondly, we have the infrared contribution of Earth to the particle, $\dot{q}_{E/IR}$,

$$\dot{q}_{E/IR} = \sigma F_E A_c \varepsilon_E \varepsilon_{IR} (T_E^4 - T_p^4) \tag{3}$$

where σ is the Boltzmann constant, F_E is the view factor of the Earth to the particle, ε_E is the emissivity of the Earth (assumed to be a black body [15]), ε_{IR} is the IR emissivity of the particle, T_E is the temperature of the Earth (assumed to be 288 K [16]), and T_p is the temperature of the particle in Kelvin. Then we have the heat flux due to Earth's albedo effects, $\dot{q}_{E/A}$,

$$\dot{q}_{E/A} = A_c F_E \frac{S}{R_{\text{AU}}^2} \alpha a K_a \psi \tag{4}$$

where a is the Earth's albedo (0.3 ± 0.05 [15]), and $K_a = 0.664 + 0.521\rho - 0.203\rho^2$ [17], with ρ being the angular Earth radius. The parameter ψ determines whether the particle is observing a sunlit portion of the Earth; $\psi = 0$ when the subsatellite point is in nighttime and $\psi = 1$ when the subsatellite point is in daytime. Lastly, we account for the particle's own emission of energy out to space, $\dot{q}_{out}$,

$$\dot{q}_{out} = \varepsilon_{IR} \sigma A_s T_p^4 \tag{5}$$

where ε_{IR} is the IR emissivity of the particle, σ is the Boltzmann constant, A_s is the surface area of the particle in m^2. We acknowledge that our formulation of $\dot{q}_{out}$ does not account for the view factor of Earth, F_E; we will consider this in future study iterations. Due to the small size of the particles considered in this study (radius between 1 and 200 microns), we find through the derivation of a radiative Biot number, Bi_{rad}, that internal heat conduction can be neglected and lump-capacitance can be utilized. Using the resistance model of heat transfer, the radiative Biot number is found from

$$Bi_{rad} = \frac{R_{internal}}{R_{external}} = \frac{\frac{L_c}{KA_s}}{\frac{1}{h_{rad}A_s}} = \frac{h_{rad}L_c}{K} \tag{6}$$

where L_c is the characteristic length in meters, K is the thermal conductivity in W/m-K, A_s is the surface area of the particle in m^2, and the radiative heat transfer coefficient reduces to $h_{rad} = 4\sigma\varepsilon T_p^3$ W/m^2-K [18]. For a sphere, the $L_c = r/3$ where r is the particle radius in meters. For all particles and materials considered in this study, $Bi << 1$. Thus, we arrive at the thermal diffusion equation, which is the differential equation solved with the dynamics to determine particle temperature in the study,

$$\frac{\partial T}{\partial t} = \left[\dot{q}_{sun} + \dot{q}_{E/IR} + \dot{q}_{E/A} - \dot{q}_{out}\right] \frac{1}{\rho C_p V} \tag{7}$$

where ρ is the density of the particle, C_p in J/kg-K is the particle specific heat capacity, and V in m^3 is the volume of the particle. To solve the dynamical system including the dynamics and thermal model, we use an implicit Runge-Kutta method from the Radau IIA family with an adaptive time step [19].

As mentioned, the thermo-orbit coupling originates from the variation of optical properties induced from temperature change and the subsequent change in SRP induced acceleration at a specific point in the orbit cycle. The user has control over the specific hot and cold inputs to optical properties and a given critical temperature, enabling modeling of orbit energy depleting or pumping cycles. A priority of this work is to establish the design space bounds for thermochromic PMPEs, so selection of optical parameters was done based on glazing materials with operational temperature ranges that aligned with fluctuations seen in low Earth orbit environments [20]. Some materials can see over a 75% change in transmittance during transition between states [21], [22]; in this study we use an 80% change as our upper bound for variation in SRP model reflectivity.

3. IDENTIFIED PERFORMANCE METRICS

The PMPE design variables were systematically analyzed to identify the parameters that most significantly influenced the generated SRP asymmetry. This analysis concentrated on thermo-orbit modeling and did not consider factors such as debris interactions. Nevertheless, it revealed several significant observations influencing particle trajectories. The first is the influence of the particle material in the thermal portion of the model. As seen in the heat diffusion equation, all heat sources are subject to a multiplier of $\frac{1}{\rho C_p V}$. Given two particles of the same size made of different constituent core materials, the thermal variation is thus closely tied to the volumetric heat cafpacity $s(T) = \rho C_p$, which characterizes a material's ability to resist temperature change. For materials with higher $s(T)$, a particle will take longer to reach its critical temperature after emerging from eclipse, leading to a larger asymmtery in SRP. This asymmetry increases because the particle remains in its "cold" optical state for a longer period before reaching the transition temperature, resulting in a prolonged stronger or weaker reflective response. Tungsten, with $s(T) = 2.58$ MJ/Km^3, was selected as a particle candidate material in previous studies for several reasons, including its hypervelocity impact characteristics and commercial availability [5]. For use as the core in a PMPE, tungsten suffers in comparison to other materials like zirconium oxide (ZrO_2) in terms of $s(T)$. ZrO_2 is a commercially available zirconia ceramic material used in energy absorption applications [23], and importantly has a volumetric heat capacity three times that of tungsten. We found this to be directly proportional to its capability to generate asymmetric SRP post eclipse, where it outperformed tungsten by a factor of three in terms of the time spent below transition temperature post eclipse emergence. As seen in Figure 3, particle temperatures post eclipse increase more gradually for ZrO_2, leading to longer times below transition temperature.

We also found that the ideal transition temperature shows minimal variation with altitude for a fixed particle design, with changes of about 1 K. This means that the particle maintains some capability to regulate the decay rate throughout its lifetime on orbit. For a test case, we simulated a tungsten particle ($r = 50\mu$m) over varying altitudes for a single orbit as shown in Figure 4. From this plot, we can observe most readily that higher altitude gives more time between eclipse conditions and conditions with or without Earth albedo effects, meaning the temperature profile change

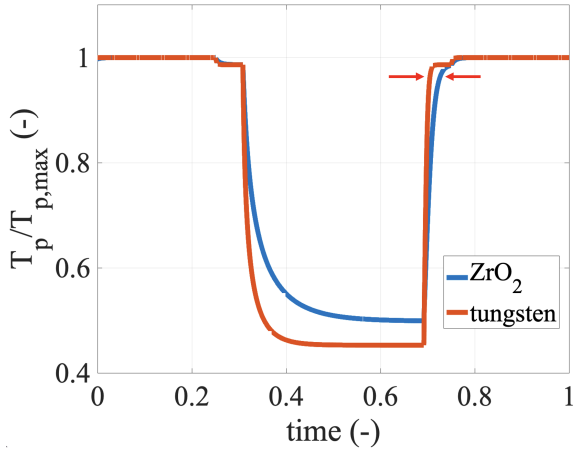

Figure 3. Particle temperatures of PMPEs with varying core materials over one orbital period, underscoring the design preference to high volumetric heat capacity constituents

is symmetric. However, higher orbits give lower peak temperatures due to the smaller view factor of Earth with increased distance, leading to a diminished contribution from Earth IR heating. Regardless, the hot-case, steady-state temperatures remain within 1-2 K of each other, as do the ideal transition temperatures. We will explore this effect in greater detail in the next section.

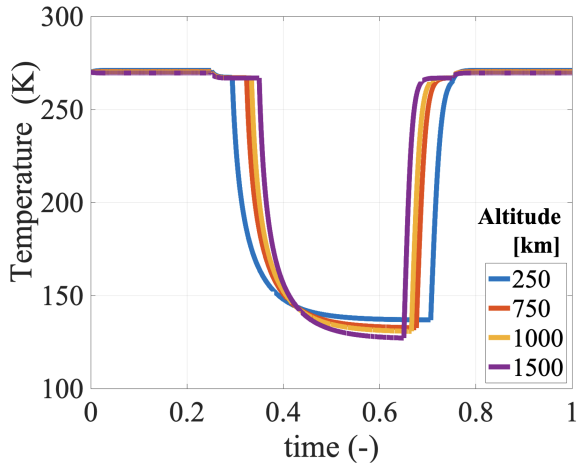

Figure 4. Particle temperature of tungsten PMPEs ($r = 50\mu$m) with varying altitude over one orbital period

Lastly, we find that with increasing particle size comes a greater ability to generate asymmetry in SRP. Shown in Figure 5, we note that there is a longer time required for the particle to reach equilibrium. This occurs because larger particles of the same material simply have a higher heat capacity. The lumped-capacitance model holds for the particle sizes shown here, partially because these particles are still quite small being below 200 microns, but also because tungsten has a relatively high thermal conductivity. While larger particles are indicated to be beneficial from the standpoint of orbit decay controlling SRP asymmetry, a more in-depth investigation is needed to conclude the appropriate upper bound for their size; large enough particles cease being PMPEs and simply become debris.

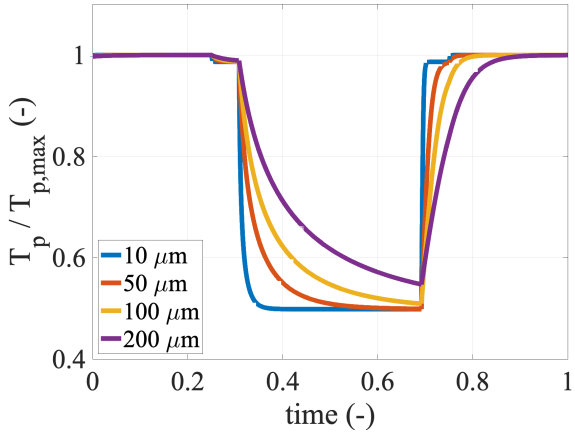

Figure 5. Varitation in temperature with varying particle radius, tungsten core PMPE, 450 km altitude, one orbital period

4. Achievable Control and Notable Effects

To analyze PMPE orbit regulating capability, we simulate a ZrO_2 ($r = 50\mu$m) particle core with varying reflectivity transitions at 267 K for orbit energy depleting and pumping cycles. While PMPEs are expected to operate in the 800 to 1000 km range, where most small debris is expected to reside [2], we investigate particle capabilities at 600, 800, and 1000 km. The results are presented in terms of the instantaneous decay or raise rate, evaluated over five days for each combination of reflectivity and altitude tested. Steeper slopes in the relationship between semi-major axis variation rate and reflectivity indicate more effective PMPEs; our analysis revealed that this relationship is linear at any given altitude within the bounds of the analyzed optical properties. The average decay rates are computed over 5 periods so we can evaluate the achievable control during solar minimum, mean, and maximum activity, which drive atmospheric density variation over the solar cycle. While total solar irradiation at 1 AU also varies with solar cycle, we do not capture these variations because they are far smaller in comparison to those seen in atmospheric density [24], [25]. Diurnal heating cycles lead to an expansion of the Earth atmosphere towards the sun during the day, resulting in significant increases in density above 300 km [26], [27]. We found that PMPEs encounter these density increases far outside of regions of induced reflectivity change. Because particle optical transitions occur relatively shortly after emerging from eclipse, diurnal heating has little effect on PMPE operations; this timing is shown in Figure 6.

Figure 7 illustrates the decay rate of particles under mean solar conditions, with a focus on those that either increase reflectivity (leading to orbital energy dissipation) or decrease reflectivity (resulting in orbital energy absorption) during their transitions from hot to cold states. Cycles involving energy absorption are depicted to the left of the zero-reflectivity variation line, while energy dissipation cycles are shown to the right. The effects of altitude are immediately apparent, with the higher drag at 600 km resulting in significantly greater decay rates compared to the 800 km and 1000 km orbits. Notably, PMPEs in orbits above 800 km can effectively "break even," where their decay rates due to atmospheric drag are counterbalanced by SRP asymmetry. At these altitudes, PMPEs can even raise their orbits if their thermochromic coating provides a sufficient boost in

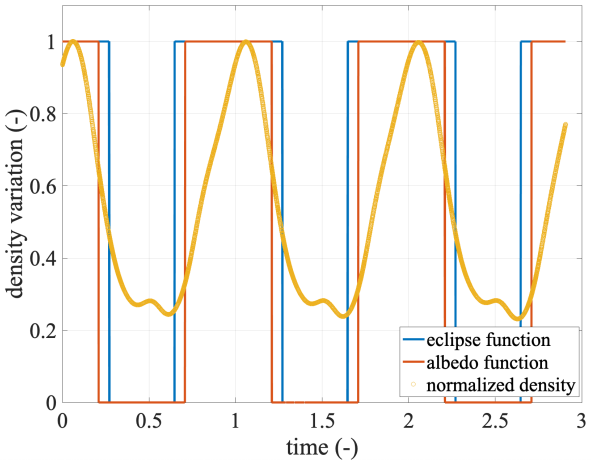

Figure 6. The timing of emergence from eclipse and nighttime subsatellite point conditions for the PMPE with variations in atmospheric density. When the eclipse and albedo functions are equal to one, the particle is in sunlight over a sunlit region of Earth. Peak atmospheric density occurs when the particle is nearly directly between the Sun and Earth.

reflectivity. While extreme variations in optical properties are rare among candidate materials in this design space, more modest reflectivity changes like ±40% still have the potential to lead to over 50% increases or decreases in decay rate over inert particles. For particles that gain 40% reflectivity during hot-to-cold transitions at 800 km, this results in the expected decay rate decreasing from about 100 m/day to 50 m/day.

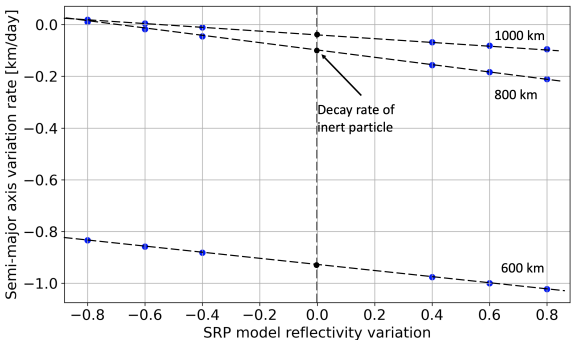

Figure 7. Decay rate in km/day under mean solar conditions (solar data from March 2016), ZrO_2, r = 50μm, 267 K transition temp, $\varepsilon_{IR} = .6$, $\alpha = .5$

PMPE control suffers in altitudes 600 km and below, where even the largest reflectivity changes only translate to the ability to raise or lower the decay rate by about 10% in comparison to inert particles. Despite no change in SRP generation between varying solar conditions, challenges in the 600 km regime are exacerbated during solar maximum, where capability falls to variations below 5% of the expected decay rate, resulting from the increase in impact of atmospheric drag. In the higher orbits considered here, decay rate control remains highly effective even under maximum solar conditions. At 1000 km, PMPEs can still raise their orbits, completely counteracting the effects of drag or doubling the decay rate, depending on the desired outcome. Compared to mean solar conditions, performance reductions are notable but not severe at 800 km, where PMPEs can still induce variation of about 30% from the expected decay rate with reflectivity changes of ±40%. Under solar minimum conditions, decay rate control increases due to reduced atmospheric density. Strong performance is noted at 800 km and above, where reflectivity changes of 40% can raise particle orbits, cancel out natural decay rates, or more than double the rate of descent. At 600 km, PMPE decay rate control capability is comparable to what was observed at 800 km under solar maximum conditions; rates for solar minimum and maximum conditions are shown in Figure 8. Satisfactory control at the target altitude of 800 km is achievable for all solar conditions and reflectivity changes tested here. The variation in decay rate control between cycles suggests that there is an optimal window during each solar cycle depending on the desired effect from the PMPEs; we leave this analysis for a future study. Mapping of the required optical property variations from our design space studies to real materials is a challenge we are currently undertaking; we note that there is promise in materials used for smart-window applications like vanadium oxides and liquid crystals [28].

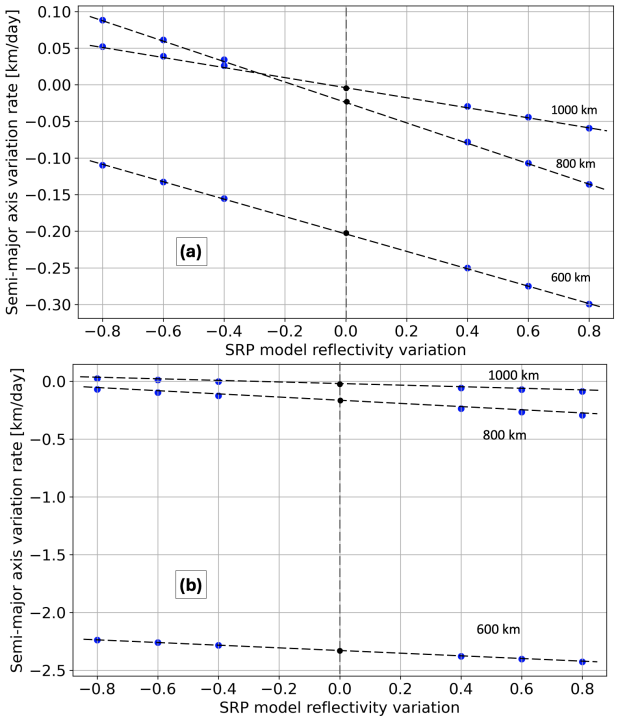

Figure 8. decay rate in km/day under a.) minimum solar conditions (solar data from August 2008), and b.) maximum solar conditions (solar data from June 2014) ZrO_2, r = 50μm, 267 K transition temp, $\varepsilon_{IR} = .6$, $\alpha = .5$

Some of the observed decline in performance at lower altitudes can be attributed to the increased effects of atmospheric drag. However, another contributing factor is the slight variations in the optimal transition temperature of the thermochromic materials used. In our constant temperature analysis, we were able to make direct decay rate comparisons by eliminating temperature variability as a factor. This approach helped isolate the effects of altitude on performance, but it also highlights the importance of tailoring particle design to specific operational altitude ranges. As seen in Figure 8(a), inducing orbit raising or enhancing decay rates is more effective at 800 km than 1000 km. While we mentioned that there was only minor variability in the optimal transition temperature with altitude (around 1-2 K), the effects of this

variability are magnified under solar minimum conditions where PMPEs gain enhanced control in the absence of more substantial drag. This implies that just as timing of particle release with the solar cycle should be optimized for a given mission profile, transition temperature should be engineered with a specific orbit range in mind. Shown in Figure 9, we see the variation in decay rate control with transition temperature from 265 K to 269 K. For this particle, the optimal transition temperature is near 266 K, where maximum control is achieved. The optimal transition temperature decreases by 1 K between 600 km and 1000 km orbits, from 267 K to 266 K. This decrease can be directly linked to the reduction in maximum temperature reached by the particles, which is a result of the slightly diminished heat contribution from Earth's IR radiation at higher altitudes. Regardless, the PMPE still maintains effective control on its decay rate in the regimes studied.

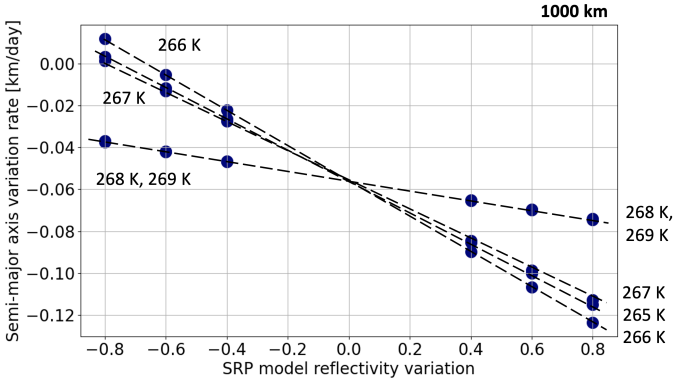

Figure 9. **Decay rate in km/day with varying transition temperature ZrO_2, $r = 50\mu$m, 1000 km orbit, $\varepsilon_{IR} = .6$, $\alpha = .5$**

5. Conclusion

Here, we have introduced the concept of Programmable Metamaterial Particle Ensembles (PMPEs) for the remediation of small debris and initiated exploring their design space, limitations, and ability to regulate orbital decay rates. Existing concepts for such remediation include the orbital or sub-orbital deployment of a dust cloud that enhances the decay rates of the debris resident in altitudes near 800 km and above. We posit that the integration of thermochromic coatings or materials into these particles will enable operators to passively control the decay rate of their cloud, significantly increasing the design space in the process; particle size selection is less constrained by the desired decay rate of the cloud, but still linked to the ideal critial temperature. We developed a thermo-orbit model to allow us to identify crucial design parameters for successful particle engineering, finding that PMPEs maintain decay rate control at a range of sizes, materials, altitudes of interest, and solar conditions. At the target altitude of 800 km, coatings with large reflectivity changes have the potential to completely cancel out or double the natural decay of the same particle without a thermochromic coating. Future work on PMPEs will identify candidate designs and determine their surviability in Earth orbital environments, add fidelity to the current thermo-orbit model, and analyze the dynamics and degradation factors of the cloud as a whole. Such factors will include decreases in cloud density due to interactions with debris and spacecrafts and expansion of the cloud due to a variety of dispersal mechanisms.

Acknowledgments

This material is based upon work supported by NASA under award #80NSSC24K0674.

References

[1] D. T. S. Kelso, "Analysis of the 2007 chinese asat test and the impact of its debris on the space environment."

[2] T. J. Colvin, J. Karcz, and G. Wusk, *Cost and Benefit Analysis of Orbital Debris Remediation*, Mar. 2023, nTRS Author Affiliations: National Aeronautics and Space Administration, Ames Research Center NTRS Document ID: 20230002817 NTRS Research Center: Headquarters (HQ). [Online]. Available: https://ntrs.nasa.gov/citations/20230002817

[3] J. Locke, T. J. Colvin, L. Ratliff, A. Abdul-Hamid, and C. Samples, *Cost and Benefit Analysis of Mitigating, Tracking, and Remediating Orbital Debris*, May 2024, nTRS Author Affiliations: National Aeronautics and Space Administration, Stevens Institute of Technology, Logistics Management Institute (United States) NTRS Document ID: 20240003484 NTRS Research Center: Headquarters (HQ). [Online]. Available: https://ntrs.nasa.gov/citations/20240003484

[4] NASA, "Civil space shortfall ranking," Jul. 2024. [Online]. Available: https://www.nasa.gov/spacetechpriorities/

[5] G. Ganguli, C. Crabtree, L. Rudakov, and S. Chappie, "Active debris removal by micron-scale dust injection," in *2012 IEEE Aerospace Conference*, Mar. 2012, p. 1–9. [Online]. Available: https://ieeexplore.ieee.org/document/6187074

[6] C. Crabtree, M. Zedd, G. Ganguli, L. Rudakov, and L. Healy, "Formation and dynamics of an artificial ring of dust for active orbital debris removal," in *2013 IEEE Aerospace Conference*, Mar. 2013, p. 1–12. [Online]. Available: https://ieeexplore.ieee.org/document/6497397

[7] G. Ganguli, C. Crabtree, A. Velikovich, L. Rudakov, and S. Chappie, "Active removal of orbital debris by induced hypervelocity impact of injected dust grains," *AIP Conference Proceedings*, vol. 1582, no. 1, p. 79–92, Feb. 2014.

[8] M. Ferrara and M. Bengisu, *Materials that Change Color - Smart Materials Intelligent Design*, Nov. 2014.

[9] S. Bender, "st-bender/pynrlmsise00," Sep. 2024. [Online]. Available: https://github.com/st-bender/pynrlmsise00

[10] J. M. Picone, A. E. Hedin, D. P. Drob, and A. C. Aikin, "Nrlmsise-00 empirical model of the atmosphere: Statistical comparisons and scientific issues," *Journal of Geophysical Research: Space Physics*, vol. 107, no. A12, pp. SIA 15–1–SIA 15–16, 2002.

[11] NOAA and NWS, "Solar cycle progression — noaa / nws space weather prediction center." [Online]. Available: https://www.spaceweather.gov/products/solar-cycle-progression

[12] D. A. Vallado, *Fundamentals of Astrodynamics and Applications*. Springer Science Business Media, Jun. 2001, google-Books-ID: PJLlWzMBKjkC.

[13] M. Cerf, "Fast solution of minimum-time low-thrust transfer with eclipses," *Proceedings of the Institution of*

Mechanical Engineers, Part G: Journal of Aerospace Engineering, vol. 233, no. 7, p. 2699–2714, Jun. 2019.

[14] G. Kopp and J. L. Lean, "A new, lower value of total solar irradiance: Evidence and climate significance," *Geophysical Research Letters*, vol. 38, no. 1, 2011.

[15] NASA, "Gd-ap-2301 - earth orbit environmental heating." [Online]. Available: https://extapps.ksc.nasa.gov/Reliability/Documents/PreferredPractices/2301.pdf

[16] "Spenvis satellite irradiation." [Online]. Available: https://www.spenvis.oma.be/help/background/ illumination/illumination.html

[17] C. D. Brown, *Elements of Spacecraft Design*. American Institute of Aeronautics and Astronautics, Incorporated, 2002, google-Books-ID: bvhTAAAAMAAJ.

[18] I. Tosun, *Modeling in Transport Phenomena: A Conceptual Approach*. Elsevier, Jul. 2007.

[19] E. Hairer and G. Wanner, *Solving Ordinary Differential Equations II*, ser. Springer Series in Computational Mathematics. Berlin, Heidelberg: Springer, 1991. [Online]. Available: http://link.springer.com/10.1007/978-3-662-09947-6

[20] L. H. R. . T. Products, "Tlc products for use in research and testing applications," no. RT001 Rev 02 P.

[21] X.-H. Li, C. Liu, S.-P. Feng, and N. X. Fang, "Broadband light management with thermochromic hydrogel microparticles for smart windows," *Joule*, vol. 3, no. 1, p. 290–302, Jan. 2019.

[22] Y. Zhou, Y. Cai, X. Hu, and Y. Long, "Temperature-responsive hydrogel with ultra-large solar modulation and high luminous transmission for "smart window" applications," *Journal of Materials Chemistry A*, vol. 2, no. 33, p. 13550–13555, Jul. 2014.

[23] AstroMet, "Zirconium oxide - amzirox 86 zirconia ceramic: Astromet." [Online]. Available: https://www.astromet.com/zirconia-amzirox86.htm

[24] T. Dudok de Wit, G. Kopp, C. Fröhlich, and M. Schöll, "Methodology to create a new total solar irradiance record: Making a composite out of multiple data records," *Geophysical Research Letters*, vol. 44, no. 3, p. 1196–1203, 2017.

[25] W. K. Schmutz, "Changes in the total solar irradiance and climatic effects," *Journal of Space Weather and Space Climate*, vol. 11, p. 40, 2021.

[26] H. K. Kallmann-Bijl and W. L. Sibley, "Diurnal variation of temperature and particle density between 100 km and 500 km," *Planetary and Space Science*, vol. 11, no. 12, p. 1379–1394, Dec. 1963.

[27] A. D. Anderson, "A simple model for atmospheric density variations from 200 to 800 km," May 1962.

[28] D. Wang, G. Chen, and J. Fu, "Multifunctional thermochromic smart windows for building energy saving," *Journal of Materials Chemistry A*, vol. 12, no. 22, p. 12960–12982, 2024.

BIOGRAPHY

Joseph Ivarson *received his Bachelor of Mechanical Engineering from the University of Dayton and his M.S. in aerospace from Auburn University where he is a 2nd year PhD student. He is currently a member of the 3i Space Dynamics Lab under the supervision of Dr. Davide Guzzetti, where he works on advanced concepts that attempt to expand capabilities in space using smart materials. He also is a NASA Space Grant Fellow and NASA Pathways Intern at Langley Research Center, where he works in the mechanics discipline of the Structural and Thermal Systems Branch.*

John Mulvaney *is an aerospace engineer with the Systems Analysis and Concepts Directorate at NASA Langley Research Center. His work is focused on capturing the current state of the art of In-space Servicing, Assembly, and Manufacturing (ISAM) technologies and analysis for use of these concepts in future in-space architectures. John serves as a research collaborator with Auburn University in support of their 2023 NASA ECF grant under Dr. Davide Guzzetti. John holds a bachelor's degree in aerospace engineering from Virginia Tech.*

Andrew Sais *is an aerospace engineer with the Systems Analysis and Concepts Directorate at NASA Langley Research Center. His work is focused on refining the process and decisions for developing an initial crew segment Mars mission architecture as well as supporting work with the NASA science and technology community to determine strategic level prioritization of Artemis utilization activities. Andrew serves as a research collaborator with Auburn University in support of their 2023 NASA ECF grant under Dr. Davide Guzzetti. Andrew holds a bachelor's degree in aerospace engineering from the Ohio State University and a master's degree in space systems engineering from the University of Michigan.*

Dr. Davide Guzzetti *is an assistant professor in the Department of Aerospace Engineering at Auburn University. Dr. Guzzetti's research focus is astrodynamics and space mission design in complex space environments, which is integrated with developing corresponding educational programs. Dr. Guzzetti has been recognized as NASA 2023 Early Career Faculty, NIAC 2020 fellow, an Auburn University Outstanding Graduate Student Mentor, and an alumnus of the Italian honor society Alta Scuola Politecnica. He is also a current member of the Space Flight Mechanics Committee of the American Astronautical Society. He obtained a Ph.D. in astrodynamics from Purdue University in 2016.*